THE JOURNAL OF PHYSICAL CHEMISTRY B

ARTICLE

pubs.acs.org/JPCB

Deswelling Kinetics of Color Tunable Poly(*N*-Isopropylacrylamide) Microgel-Based Etalons

Matthew C. D. Carter, Courtney D. Sorrell, and Michael J. Serpe*

Department of Chemistry, University of Alberta, Edmonton, AB T6G 2G2, Canada

Supporting Information

ABSTRACT: Poly(*N*-isopropylacrylamide) (pNIPAm) microgel-based etalons are optical materials fabricated by depositing a monolithic layer of microgels on a semitransparent Au film adhered to a glass coverslip, followed by the deposition of a second semitransparent Au layer over the microgel layer (overlayer). These materials exhibit characteristic colors and multipeak reflectance spectra, both of which depend on the distance between the Au surfaces (mediated by the microgel diameter) and the refractive index of the microgel layer. In this submission, the deswelling kinetics of pNIPAm microgel-based etalons are investigated by inducing microgel deswelling through exposure to a 30% methanol/H_2O solution. Exposed to this solvent system, the transition temperature of the microgels is lowered to a temperature below the experimental temperature and the microgels comprising the etalon collapse. This collapse induces an etalon color change, which is observed as a blue shift in the reflectance spectrum. The kinetics of deswelling were shown to be strongly dependent on the thickness of the Au overlayer, e.g., thicker overlayers slow the solvent exchange and the resultant deswelling kinetics. Additionally, for thicker overlayers, the rate of deswelling increases with decreasing etalon size. Taken together, these results suggest that the kinetics depend strongly on the ability of the solvent to exchange from/to the microgel layer. For example, if the Au overlayer is thin, more solvent can exchange through the overlayer in a given amount of time compared to an etalon composed of a thick overlayer. Likewise, etalons of smaller dimensions have faster deswelling kinetics due to the shorter distance the solvent needs to travel laterally through the microgel layer to exchange. The results from this study are of fundamental importance but will be used to develop sensors with fast response times for point-of-care diagnostics.

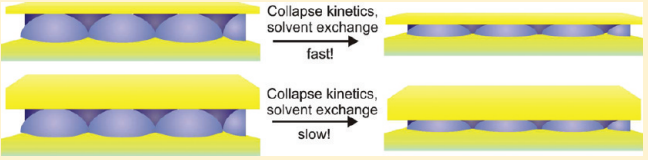

INTRODUCTION

Point-of-care (POC) diagnostics have become increasingly important for disease diagnosis, especially in economically strained regions because they are often inexpensive, portable, simple to manufacture and use, require little to no sample preparation, and can be engineered to be extremely sensitive.[1−3] Moreover, they have the added benefit of not requiring spectroscopic equipment for determining the result of the test, i.e., the result of the test is often read out visually.[4,5] Typical sensors of this type have been developed to detect early pregnancy,[6] blood glucose levels,[7] drug screening,[5] and various disease biomarkers.[8,9] Detection of these analytes often requires a sensitive device that can distinguish an analyte from within a complex solution; therefore, new materials are in development in order to enhance POC and diagnostic sensing.

Photonic materials are an interesting class of optical materials that can interact with incident light to produce color. These materials are fabricated by assembling structures of contrasting refractive indices into some ordered arrangement. Previously, these materials have been used for biosensing,[10,11] coatings,[12] and as light filters.[13,14] A relatively simple example of an optically active photonic material is the Fabry−Pérot etalon (etalon). An etalon is composed of two planar mirrors separated by a dielectric cavity; these materials are considered one-dimensional photonic materials.[15,16] Light impinging on the surface of the first mirror−dielectric interface splits into a reflected beam and a transmitted beam. The transmitted beam passes through the dielectric layer, eventually striking the second mirror, resulting once again in a reflected and transmitted beam. The light continues to resonate in the dielectric cavity, resulting in constructive and destructive interference and in specific wavelengths of light being selectively reflected and transmitted. The result is a multipeak reflectance spectrum for an etalon, and visible color is observed. The wavelengths of light reflected depend on the distance between the mirrors of the etalon and on the refractive indexes of the dielectric layer according to eq 1,

$$\lambda = \frac{2nd\cos\theta}{m} \quad (1)$$

where n is the refractive index of the dielectric layer, d is the mirror−mirror distance, θ is the angle of incident light relative to the normal, and m, an integer, is the order of the reflected peak.[15,16] Etalons and similar one-dimensional materials could be used for POC sensing, but in order to develop sensors of this type, one must employ a responsive material that can induce a change as a function of some stimulus.[10,17,18]

Received: July 26, 2011
Revised: September 24, 2011
Published: October 26, 2011

Recently, our group reported on color tunable etalons composed of temperature responsive poly(*N*-isopropylacrylamide) (pNIPAm) microgels.[19−21] PNIPAm microgels have been extensively studied, and when heated to $T > \sim 32$ °C in aqueous solution, they are well-known to decrease their size (deswell). Microgels expel their water of solvation as a result of this transition, which has been shown to be fully reversible. Therefore, when $T < \sim 32$ °C, the microgels reswell with water and increase their diameter.[22−24] The temperature at which the microgel size transition occurs is termed the volume phase transition temperature (VPTT).

The efforts of many groups have proven microgels to be an appealing platform for sensing purposes because they can be easily engineered to swell/deswell in response to various stimuli. That is, through the use of functional comonomers, microgels that respond to various stimuli can be synthesized. For example, acrylic acid (AAc) is a common comonomer that renders pNIPAm microgels responsive to pH and provides a site to which further functionality can be added.[13] Interestingly, pNIPAm-based materials have also been generated that respond to glucose,[25] protein binding,[26] and DNA hybridization.[27]

Our group generates color tunable materials by sandwiching pNIPAm-*co*-AAc microgels between two thin gold (Au) films; hence, the mirror−dielectric−mirror motif common to an etalon is created.[19,20] These microgel-based etalons can be fabricated to have a characteristic color (both visually and spectrally), and because the microgels exhibit a diameter that is dependent on temperature and pH, the mirror−mirror spacing can be dynamically tuned. The result is color tunability according to eq 1. It should be noted here that while refractive index can lead to color shifts, the color for these systems is dominated by the change in the mirror−mirror spacing.[19,20] These materials exhibit multipeak spectra that shift > ∼300 nm spectrally in response to an increase in temperature of ∼15 °C. This high sensitivity makes microgel-based etalons excellent platforms for optical sensing applications. By incorporating microgels that undergo a diameter change in response to the presence of an analyte, the mirror−mirror distance, and hence color will depend on the presence or absence of a specific analyte. While the response from these materials is extremely sensitive, we wish to develop sensors that also exhibit fast response times that would be appealing for POC applications.

To develop such sensors, it is important to understand the mechanism by which an etalon actuates. An analyte must enter the etalon and make contact with the microgel dielectric layer; next, the microgels must respond by swelling/deswelling; these processes require a solvent exchange between the dielectric layer and the bulk solvent. Therefore, the response time must depend on both (1) how quickly the analyte can enter the dielectric cavity; and (2) how quickly the microgels change their solvation state while confined within the cavity, which is dependent on how freely the solvent can exchange with the bulk solution. While the latter depends partially on physical or chemical interactions between the microgels and the analyte, and is therefore analyte specific, much of the response is dependent on the physical structure of the etalon assembly. Currently, microgel etalons are built on glass slides, so the entry of analytes through this bottom face is blocked. However, the edges of the etalon are open, and a thin Au overlayer forms the top face. Therefore, we hypothesize that solvent exchange (and analyte entry) may proceed through the sides and the top of the etalon. Here, we probe the deswelling kinetics of microgel etalons, and we show that the rate at which etalons deswell depends strongly on the Au overlayer thickness. The results reveal that the etalons exchange with their solvent primarily through the Au overlayer; however, some activity through the edges can be observed. Consequently, an etalon with a thin Au overlayer responds faster than an etalon with a thick Au overlayer. Furthermore, an etalon with small dimensions generally responds faster than an etalon with large dimensions; although when the overlayer is thin there is minimal exchange laterally through the microgel layer, and therefore, the etalon size has virtually no effect on the deswelling kinetics. Therefore, a responsive etalon with a thin Au overlayer would be ideal for colorimetric POC sensing.

EXPERIMENTAL SECTION

Materials. *N*-Isopropylacrylamide was purchased from TCI (Portland, Oregon) and purified by recrystallization from hexanes (ACS reagent grade, EMD, Gibbstown, NJ) prior to use. *N*,*N*′-methylenebisacrylamide (BIS) (99%), acrylic acid (AAc) (99%), and ammonium persulfate (APS) (98+%) were obtained from Sigma-Aldrich (Oakville, Ontario) and were used as received. Sodium chloride for adjusting ionic strength was obtained from EMD and was used as received. All deionized (DI) water was filtered through a Milli-Q Plus System (Millipore, Billerica, MA) to have a resistivity of 18.2 MΩ·cm. Chromium/gold annealing was done in a Thermolyne muffle furnace from Thermo Fisher Scientific (Ottawa, Ontario). Anhydrous ethanol was obtained from Commercial Alcohols (Brampton, Ontario). Methanol (MeOH, 99.8%) and hydrochloric acid were purchased from Caledon Chemicals (Georgetown, Ontario) and were used as received. Fisher's Finest glass coverslips were 25 × 25 mm and obtained from Fisher Scientific (Ottawa, Ontario). Chromium and gold were 99.999% and obtained from ESPI (Ashland, OR).

Microgel Synthesis. Microgels composed of poly(*N*-isopropylacrylamide-*co*-acrylic acid) (pNIPAm-*co*-AAc) were synthesized via temperature-ramp, surfactant free, free radical precipitation polymerization as described previously.[28] The monomer mixture, with total concentration of 154 mM, was comprised of 85% *N*-isopropylacrylamide (NIPAm) and 10% acrylic acid (AAc) with a 5% *N*,*N*′-methylenebisacrylamide (BIS) cross-linker. The monomer, NIPAm (8.5 mmol), was dissolved in deionized water (50 mL) with stirring in a small beaker. The mixture was filtered through a 0.2 μm filter affixed to a 20 mL syringe into a 100 mL 3-neck round-bottom flask. The beaker was rinsed with 12.5 mL of deionized water and then filtered into the NIPAm solution. The flask was then equipped with a temperature probe, a condenser and N_2 outlet, stir bar, and a N_2 gas inlet. The monomer solution (62.5 mL total volume) was purged with N_2 gas for about 1 h, with stirring set to a rate of 450 rpm, while the temperature was allowed to reach 45 °C. AAc (1.0 mmol) was then added to the heated mixture with a micropipet. A 0.078 M aqueous solution of APS (2.5 mL) was delivered to the monomer solution with a transfer pipet to initiate the reaction (total reaction volume 65.0 mL). Immediately following initiation, a temperature ramp of 45 to 65 °C was applied to the solution at a rate of 30 °C/h, and a 5 mL solution of BIS (0.50 mmol) in deionized water was then dripped into the solution over the course of the temperature ramp (∼45 min). Following the completion of the ramp and introduction of the cross-linker, the reaction was allowed to proceed overnight at 65 °C. After polymerization, the reaction mixture was filtered

through glass wool to remove any large aggregates. The coagulum was rinsed with deionized water, and the solution was diluted to ~120 mL (diluted approximately two times from the original microgel solution concentration). Aliquots of these microgels (12 mL) were centrifuged at a speed of ~8400 relative centrifugal force (rcf) at 23 °C to produce a pellet at the bottom of the centrifuge tube. The supernatant was removed from the pellet of microgels, which was then resuspended to the original volume (12 mL) using deionized water. This process was completed a total of six times to remove any unreacted monomer and/or linear polymer from the microgel solution.

Etalon Fabrication. The details of the paint-on technique used to fabricate microgel etalons for these experiments have been reported previously.[20] Briefly, 25 × 25 mm glass coverslips were rinsed with ethanol and dried with N_2 gas, and 2 nm of Cr followed by 15 nm of Au were thermally evaporated onto them at a rate of ~1 Å s^{-1} and ~0.2 Å s^{-1}, respectively, using a Torr International Inc. model THEUPG thermal evaporation system (New Windsor, NY). The Au coated substrates were annealed at 250 °C for 3 h and then cooled to room temperature by removing the slides from the oven. An aliquot of about 12 mL of microgel solution was centrifuged for 30 min at 23 °C at ~8400 relative centrifugal force (rcf) to pack the microgels into a pellet. A Cr/Au substrate was rinsed with ethanol, dried with N_2, and then placed onto hot plate (Corning, NY) set to 30 °C along with the tube containing the microgel pellet for ~5 min. A 40 μL aliquot of the concentrated microgels was deposited onto the substrate and then spread toward each edge using the side of a micropipet tip. The film was rotated 90°, and the microgel solution was spread again. The spreading and rotation continued until the microgels covered the entire substrate. The microgels were allowed to dry completely on the substrate for 2 h with the hot plate set to 35 °C. After 2 h, the dry film was rinsed with deionized water to remove any excess microgels not bound directly to the Au. Next, the film was placed into a deionized water bath and allowed to incubate overnight on a hot plate set to ~30 °C. Following this step, the substrate was again rinsed with DI water to further remove any microgels not bound directly to the Au substrate surface. Following this rinsing step, the film was dried with N_2 gas and placed into the metal evaporator, and an additional 2 nm Cr followed by the desired Au overlayer thickness was deposited onto the microgels as an overlayer. These assemblies, now formally etalons, were soaked in DI water overnight on a hot plate set to ~30 °C and subsequently used for experiments.

When smaller etalons were required, a full-size 2.5 × 2.5 cm etalon fabricated as above was carefully cut to size by hand using a Fisherbrand diamond pencil.

Reflectance Spectroscopy. Reflectance measurements were conducted using a USB2000+ spectrophotometer, a HL-2000-FHSA tungsten light source, and a R400-7-VIS-NIR optical fiber reflectance probe all from Ocean Optics (Dunedin, FL). The spectra were recorded using Ocean Optics Spectra Suite Spectroscopy Software over a wavelength range of 350−1039 nm. Measurements were performed in a specially designed sample holder, which allows for careful sample positioning, sample stability, solvent injection, and fine temperature control (see Supporting Information).

Atomic Force Microscopy. Images of the overlayer of the 5 and 35 nm overlayer etalons from set 1 used in this study were acquired using an Asylum Research MFP 3D AFM (Santa Barbara, CA). Each image was acquired over 50 μm × 50 μm, 20 μm × 20 μm, 5 μm × 5 μm, 2 μm × 2 μm, and 500 nm × 500 nm areas using a scan rate of 0.54 Hz and 512 scan points and lines. The tips were Nanoworld Arrow-NCR-50 with a resonant frequency of 285 kHz.

In-liquid height analysis for an etalon in pH 3 water (2 mM IS) and a 30% MeOH solution in pH 3 water (2 mM IS) was performed using the 5 nm overlayer sample from set 1 used in this study, and the images were acquired using an Asylum Research MFP 3D AFM (Santa Barbara, CA). Images were acquired over a 50 μm × 50 μm area using a scan rate of 0.45 Hz and 512 scan points and lines. The tips were Olympus TR800PSA with a resonant frequency of 24 kHz. An image was taken using a sessile drop method first in pH 3 water at ~25 °C, followed by 30% MeOH in pH 3 water at an ambient chamber temperature of ~25 °C. For this analysis, a line was scratched into the sample using a new razor blade, and the scratch was imaged. The height was determined using the software by taking 100 line blocks and measuring the height on a line trace. Four 100 line blocks were measured and averaged to get an average height and standard deviation for each image (see Supporting Information).

Optical Microscopy. Microgels were diluted in pH 3 water (2 mM IS), and a droplet was placed on to a plain glass coverslip, and an image was captured. Microscope images of the films and microgels were taken using an Olympus IX71 inverted microscope (Markham, Ontario) fitted with a 100× oil-immersion objective, a 10× eyepiece, differential interference contrast (DIC) optics, and an Andor Technology iXon+ camera (Belfast, Ireland). Andor SOLIS v4.15.3000.0 software was used to record microscope images. An image of an Edmunds Industrial Optics (Barrington, NJ) PYSER-SGI scale grating (50 × 2 μm) was used to determine the scale bars.

Kinetics Studies. An etalon of a given overlayer thickness was placed in the specially constructed sample holder (see Supporting Information). Next, 24 mL of pH 3.0, ionic strength (IS) 2 mM (from NaCl addition) water was introduced through the rear port of the sample holder via a syringe. The temperature of this solution was maintained at 25 °C. The solution was also stirred at a constant rate for each experiment, and the spectrum was monitored in real time. The intensity of the light source was set to result in a clear spectrum with intense reflectance peaks between 80−100% reflectance. Individual spectra were an average of two scans at 100 ms intervals. The etalons were allowed to stabilize in the sample holder until the reflectance peaks ceased shifting. This often took ~1 h. A solution of methanol (MeOH) in water was made by vigorously stirring together 20 mL of MeOH and about 20 mL of the aforementioned pH 3.0 IS 2 mM water for 30 min in a 50 mL volumetric flask. This step is necessary to remove any bubbles formed by the mixing of water and MeOH and to dissipate the heat of mixing. After 30 min, few bubbles remained, so the stir bar was removed magnetically, and the solution was diluted to volume with the pH 3.0 solution to yield a 40% MeOH/H_2O solution. At this time, 18 mL of the water in the sample holder was removed and replaced with 18 mL of the 40% MeOH/H_2O solution, such that the total volume in the sample holder is again 24 mL. This results in a 30% (v/v) MeOH/H_2O solution in the chamber, as intended. The zero time point of data acquisition, $t = 0$, was taken as the point at which the injected sample passed the 5 mL mark of the syringe. Spectra were saved at 1 s intervals, and the acquisition was allowed to proceed for many hours until the peaks had stopped blue shifting. This stopping point was determined by carefully monitoring the deswelling response, and after it appeared that the peaks had ceased shifting, acquisition was allowed to

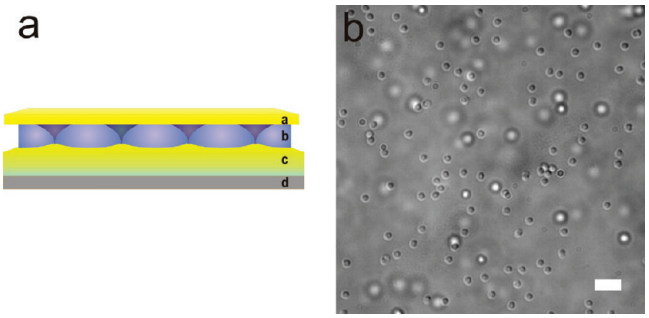

Figure 1. (a) Cartoon image of a microgel etalon depicting a and c, the reflective surfaces; b, the microgel dielectric layer; and d, the glass substrate on which microgel etalons are built. (b) DIC microscopy image of microgels used to make the etalons in the study. Microgels in the focal plane are adsorbed to a glass substrate, while the microgels out of focus (seen as circles) remain in solution above the plane of focus. The microgels are in pH 3 water (2 mM IS). The scale bar is 5 μm.

continue for about 1 h to ensure signal stability. The same process was followed for each etalon of different overlayer thickness. It is important to note that the same location, near the center of each etalon was probed. This is achieved through the use of an XY micrometer translation stage (Newport, Irvine, CA) on which the sample holder is built. When successive MeOH induced deswellings of a single etalon were required, the etalon was first removed from the sample holder and rinsed with pH 3 IS 2 water five times. In between rinses, the etalon was allowed to incubate in the water for about 15 min. After reintroduction to the sample holder, it was allowed to stabilize as above. For each etalon that was successively deswollen in the MeOH solution, the initial spectrum was nearly identical from run to run. This strongly indicates that MeOH can easily be removed from the etalon and that none remains in the microgel cavity, which could skew the results.

Kinetic parameters of interest were extracted from the acquired deswelling curves. To find the maximum rate of deswelling, the derivative of the curves was performed to find their inflection point, and then three data points on either side of the inflection point were used to fit the equation of a straight line, $y = mx + b$. The slope, m, was the maximum rate of deswelling in units of inverse seconds, s^{-1}. Additionally, deswelling curves were fit to the exponential equation, $Y = \mathrm{IF}(X < X0, Y0, Y0 + (\mathrm{Plateau} - Y0)*(1 - \exp(-K*(X - X0))))$ in Prism GraphPad 5 (La Jolla, CA), which is appropriate for fitting data of this type, where a lag phase is followed by a rise and a plateau. $X0$ was set to equal the time at the onset of the deswelling phase for each individual curve. $Y0$ is the average percent deswollen value up until $X0$, and K is the rate constant in units of s^{-1}. The plateau value was set to the constant value of 100 for all curves to represent 100% deswollen; $Y0$ was left unconstrained; and K was constrained to be a positive value. A maximum number of iterations (99999) was performed, and the Goodness of Fit value, r^2, was less than 0.9620 for only one case and was frequently greater than 0.9800.

RESULTS AND DISCUSSION

Fabrication and Experimental Considerations. Microgel-based etalons are fabricated by depositing a monolayer of microgels onto a 15 nm gold coated glass slide using a paint-on protocol.[20] Next, a gold overlayer was deposited onto the microgels via thermal evaporation, giving rise to the familiar mirror−dielectric−mirror sequence reminiscent of a Fabry−Pérot etalon; see Figure 1a. The microgels that form the dielectric cavity are jammed, and they form a monolithic layer. Microgels used in this study were composed of poly(*N*-isopropylacrylamide) (NIPAm) and acrylic acid (AAc) as a comonomer. As can be seen from the DIC microscopy image in Figure 1b, the microgels had a diameter of ∼1.5 μm and were relatively monodispersed.

Because the microgels are sandwiched between two Au layers, they are necessarily confined systems; therefore, the deswelling response should depend on the ability of the bulk solvent to access the microgel layer and the ability of the solvent in the microgel layer to be expelled. It follows that faster deswelling kinetics should be achieved with etalons that can more freely exchange solvent. Since the porosity of thermally evaporated Au has been shown to decrease with increasing thickness, it stands to reason that if solvent is being exchanged through the Au overlayer, the deswelling kinetics should decrease with increasing Au overlayer thickness.[29,30] To probe how the deswelling kinetics of our materials depend on Au overlayer thickness, etalons with six different Au overlayer thicknesses were fabricated. The nominal overlayer thicknesses studied were 5, 10, 15, 20, 25, and 35 nm.

For this study, the microgels making up the dielectric cavity of each etalon were deswollen by exploiting the cononsolvency effect.[31−34] Briefly, the phase transition temperature of pNIPAm has been shown to depend on solvent composition. That is, the addition of specific solvent/water mixtures to pNIPAm can cause the VPTT of pNIPAm to shift, making it is possible to cause microgels made up of pNIPAm to deswell at a variety of temperatures.[33,35] Here, microgel etalons were stabilized at 25 °C in pH 3.0 water with an ionic strength of 2 mM, and a MeOH/H_2O solution was added to create a 30% (v/v) MeOH/H_2O solution. At this MeOH concentration, the VPTT of the microgels decreases dramatically to ∼18 °C, so the microgels should instantly deswell.[33,35] In microgel etalons, as the microgels deswell, the Au mirrors approach each other, resulting in a spectral blue shift according to eq 1. The deswelling kinetics were monitored for etalons of different overlayer thicknesses, during two independent experiments (set 1 and set 2). All etalons in this study were constructed from the same set of microgels.

The zero time point for the experiment was the same for each etalon, and the peak at $t = 0$ is given by $\lambda_{initial}$. Zero time was defined as the point when 5 mL of the MeOH/H_2O solution remained in the injection syringe. Each etalon of different overlayer thickness does not have the same absolute shift in wavelength, λ_{total} (as discussed in detail later), so the data was normalized by plotting the percentage shift versus time. The percentage shift for a particular data point with a wavelength peak value of λ_{max} is given by eq 2,

$$\%\mathrm{shift} = \frac{\lambda_{max} - \lambda_{initial}}{\lambda_{final} - \lambda_{initial}} \times 100 \qquad (2)$$

where λ_{max} is the wavelength of the monitored peak at a particular time point, $\lambda_{initial}$ is the initial peak position, and λ_{final} is the final peak position. Because the etalons were fabricated with the same microgels and by the same fabrication method, it is an excellent assumption that the order of the observed reflection peaks, for etalons with different overlayer thicknesses, are all the

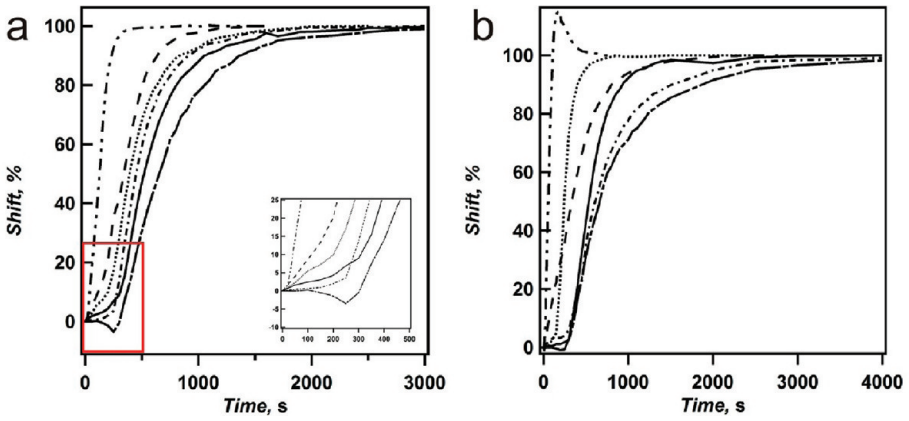

Figure 2. Deswelling curves for the etalons in (a) set 1 and (b) set 2. The percentage shift of the high wavelength peak is plotted as a function of time. Overlayer thicknesses are 5 nm (— · · —), 10 nm (— — —), 15 nm (· · ·), 20 nm (solid), 25 nm (— · —), and 35 nm (— · · —). Inset (red box in a) shows the expansion of the % shift versus time plot to highlight the lag phases. A negative % shift is observed at the highest overlayer thickness of 35 nm for the lag phase portion. This is hypothesized to be a result of the refractive index of the solution changing, without a mirror−mirror distance change, as described in the text. Deswelling was induced by introducing a 30% (v/v) MeOH/water solution (2 mM IS) held at 25 °C.

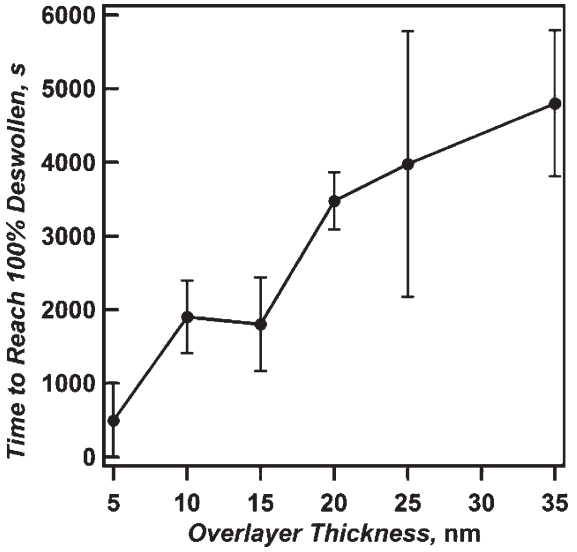

Figure 3. Time required for etalons of various overlayer thicknesses to reach 100% deswollen. Error bars are the standard deviations for the averages from two different sets of independently fabricated samples.

same. The $\lambda_{initial}$ values are slightly shifted with different overlayer thicknesses, for reasons described below. Therefore, all of the highest wavelength peaks for all the etalons will be the same order and all can be directly compared.

Deswelling Kinetics. A plot of the percentage shift versus time is given in Figure 2 for two sets of independently fabricated etalons, which have six different overlayer thicknesses. The curves can be broken into three phases: the initiation or lag phase, deswelling, and the plateau. The lag phase begins after the MeOH/H_2O solution is introduced, and during this phase, the etalons deswell slowly (with the exception of the 5 nm overlayer etalon). The deswelling phase is defined by a sharp increase in the rate of deswelling; this is the state at which the etalon most quickly expels its solvating water. The plateau phase occurs as the etalon approaches 100% deswollen.

The total time it takes for an etalon to deswell increases with increasing overlayer thickness. This is shown in Figure 3, as etalons with thicker Au overlayers require more time to reach 100% deswollen than do etalons with thinner overlayers. In fact, an etalon with a thin, 5 nm overlayer deswells in about a tenth of the time it takes the thickest etalon to deswell. Similar to the work of Norrman et al.,[29] which shows that the area of a substrate uniformly coated with Au increases with increasing thickness, AFM images of our etalons in Figure 4 reveal that 5 nm Au overlayers are more porous than the 35 nm overlayers. This allows the microgels coated with thin Au overlayers to more easily exchange solvent when undergoing a transition compared to microgels covered with thicker Au overlayers. Thin overlayers ultimately lead to faster deswelling kinetics as there are more opportunities for the solvent to exchange through both the sides and the top of the etalon. In sensing terms, the data suggests that an analyte (simulated here by MeOH) comes into contact with the microgel layer primarily via diffusion through the Au overlayer. This is evident from Figure 2, as the lag phases for etalons with thicker overlayers increase relative to those with thinner overlayers. Interestingly, the etalons never fail to actuate; for the thickest overlayer of 35 nm, the microgels continue to deswell, suggesting that either solvent can exchange through the edges or that 35 nm is not entirely a bulk film that blocks the solvent exchange process.[29,30]

Note that for the data in set 1, the etalon with an overlayer thickness of 25 nm does not fit the overall trend. It appears to shift too quickly, shifting slightly faster than the 20 nm overlayer film in the deswelling phase. Typically, in replicates of this experiment, one curve does not fit the overall trend. While we are unsure why this is the case, it is likely due to slight differences inherently present in the fabrication method, which may lead to regions of the overlayer that are slightly more porous than others. As a result, if the area being observed during the deswelling experiments contains more/fewer pores relative to the rest of the film, it will skew the data accordingly. For all experiments here, the general trend of slower deswelling kinetics with increasing overlayer thickness holds (for all but one of the samples), so we are confident with formulating mechanistic hypotheses for the solvent exchange mechanism that governs the overall deswelling rate.

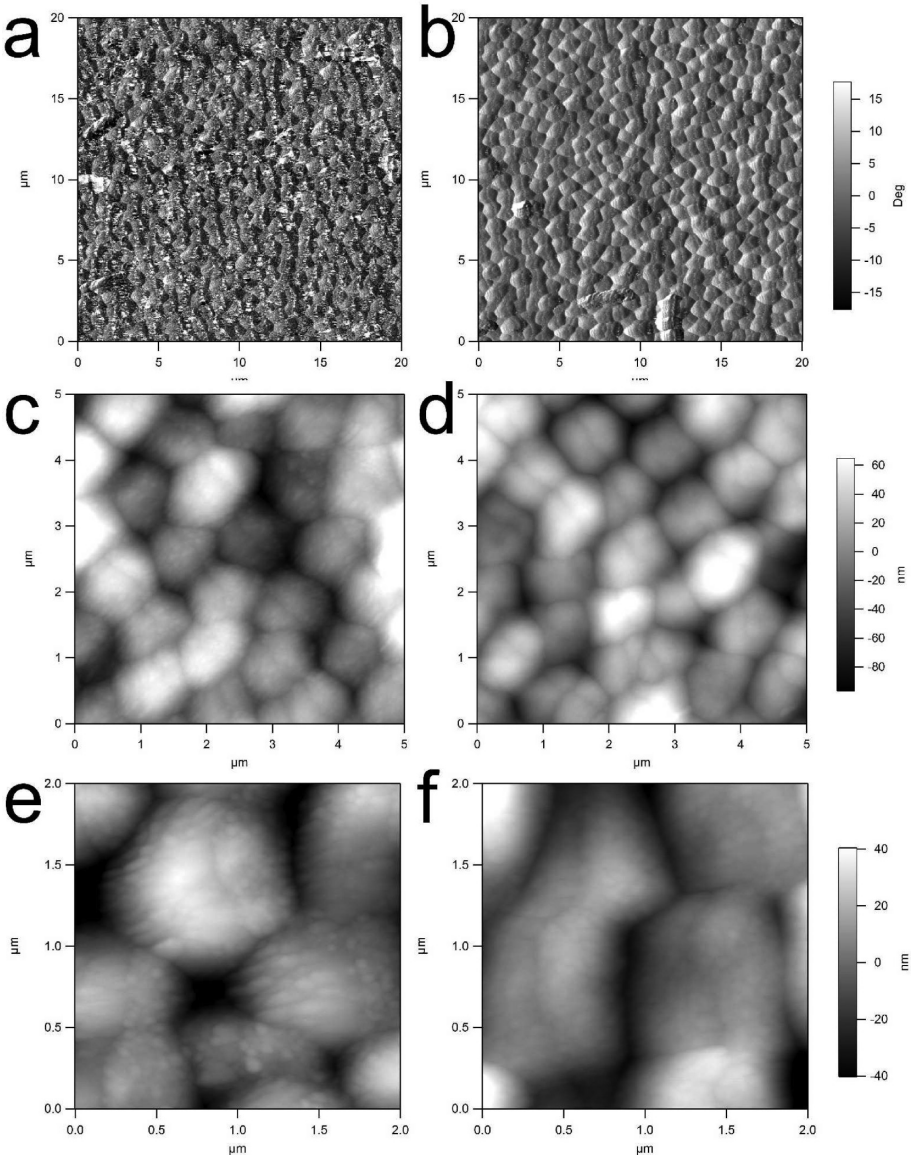

Figure 4. AFM phase images, taken using a 0° scan angle, depicting etalons from the kinetics experiments with (a) 5 nm overlayer and (b) 35 nm overlayer of Au. AFM height images, taken using a 30° scan angle, depicting the same etalon with (c) 5 nm overlayer and (d) 35 nm overlayer of Au. AFM height images, taken using a 0° scan angle, depicting the same etalon with (e) 5 nm overlayer and (f) 35 nm overlayer of Au. For all images, there is an adhesion layer of 2 nm of Cr under the Au. Z-scales are shown on the right and are the same for the images in that row. From the images, it can be seen that the 5 nm overlayer is grainier than the 35 nm overlayer, indicating more pores in the Au overlayer.

Again, the data in Figure 2 reveals that the lag phase increases with increasing overlayer thickness. This strongly supports the idea that the process of diffusion through the Au overlayer is slowed with thicker Au overlayers. Once the stimulus has made contact with the microgels, the etalon deswells relatively quickly, again, in proportion to the Au overlayer thickness. However, the plateau phase during which the microgels fully deswell also depends strongly on the overlayer thickness, increasing with overlayer thickness. As microgels deswell, they expel their water of solvation, which must leave the dielectric cavity through the overlayer or through the edges. The fact that the plateau phase time increases with increasing overlayer thickness suggests that the dominant mechanism of exit is through the overlayer.

For the thickest overlayer of 35 nm, it is sometimes possible to observe a change in the refractive index of solution during the lag phase, prior to the etalon actuating. Figure 2 (inset) reveals that the 35 nm etalon in particular undergoes an early negative percent shift. This is due to the peaks red-shifting shortly after the introduction of the MeOH/H_2O solution. We attribute this to the refractive index change of the solution, increasing from 1.3325 (water, 25 °C) to 1.3382 (30% (v/v) MeOH/H_2O; 25 °C),[36] without a mirror−mirror distance change. This behavior can be anticipated by eq 1.[37] This observation is often fleeting and may be difficult to replicate purely because the stirring rate in the experimental apparatus is only roughly constant.

Kinetic parameters of interest can be extracted from the data presented in Figure 2, e.g., maximum deswelling rate and deswelling rate constants, as explained in the Experimental Section. Figure 5a shows how the maximum deswelling rate changes with overlayer thickness. The figure reveals that the thin,

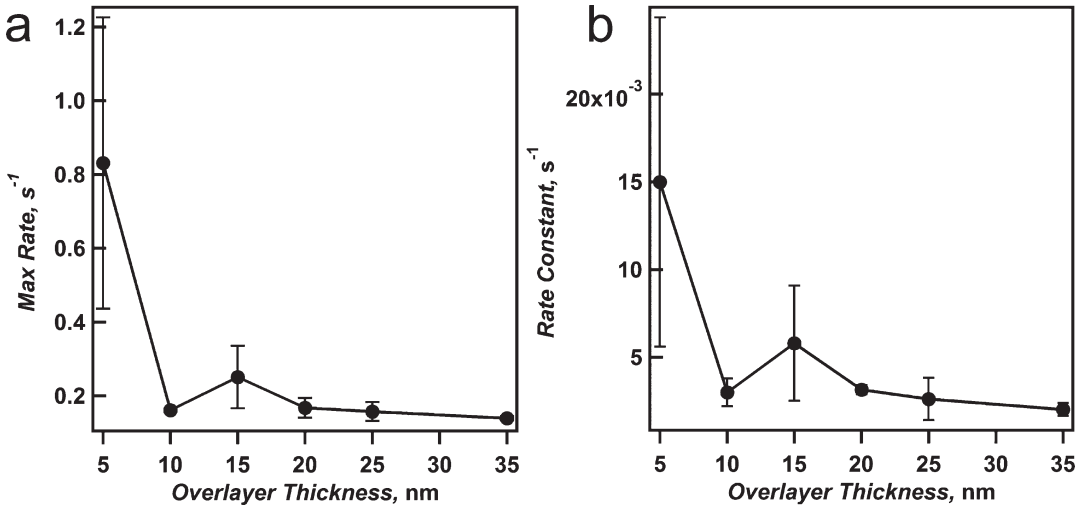

Figure 5. (a) Maximum rate of deswelling and (b) deswelling rate constant given in units of s^{-1} for etalons with different Au overlayer thicknesses. Data is presented as an average over two sets of independently fabricated etalons; error bars are the standard deviations for the averages from two different sets of samples.

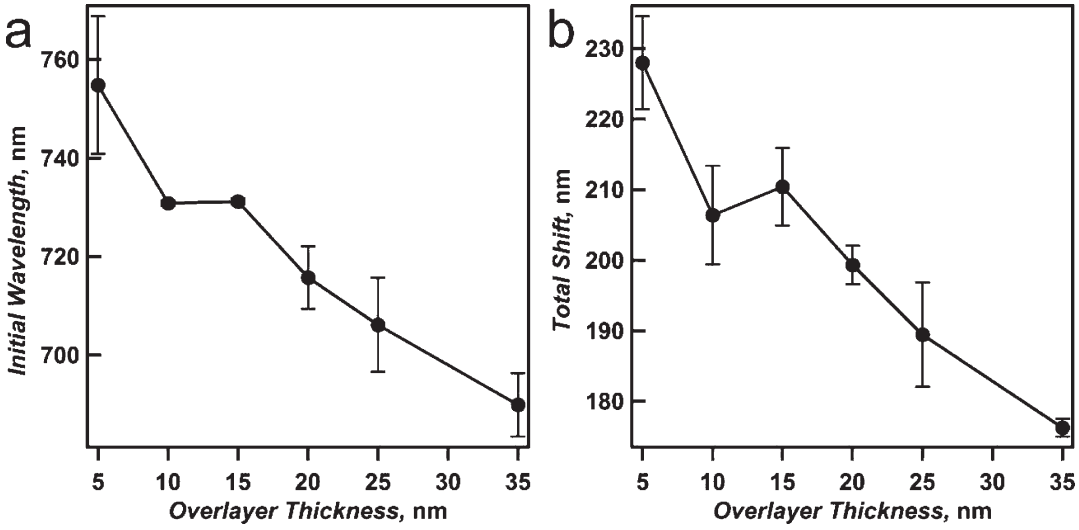

Figure 6. (a) Initial wavelength and (b) total wavelength shift for etalons with six different overlayer thicknesses. Error bars are the standard deviations for the averages from two different sets of independently fabricated samples.

5 nm Au overlayer has an enhanced maximum deswelling rate compared to etalons with thicker overlayers. Furthermore, Figure 5b reveals that the overall deswelling rate constant, determined from an exponential fit of the data (see Experimental Section), for the 5 nm Au overlayer is much greater than that of the etalons with thicker Au overlayers. The enhanced deswelling kinetics for the etalons with thin Au overlayers makes them most appealing for sensing applications.

Ideally though, microgel etalon sensors should have a fast response time, combined with high sensitivity, as evidenced by the magnitude of the wavelength shift in response to an analyte (in this case modeled by MeOH). By plotting $\lambda_{initial}$ as well as the total wavelength shift against the overlayer thickness, as in Figure 6a,b, respectively, the trend of decreased $\lambda_{initial}$ and total λ shift with increased overlayer thickness is revealed. There are multiple possibilities for the decreased $\lambda_{initial}$ with increased overlayer thickness. First, as the Au overlayer thickness increases it becomes more rigid, which can prevent the microgels from swelling as fully as microgels in etalons made with the less rigid, thin Au overlayers. Second, the increase in mass of the microgels from the thicker overlayers, relative to thinner ones, serves to compress the microgel dielectric layer, effectively making the mirror−mirror distance decrease. Regardless of the cause, the effect is the same: the spectra blue shift with increasing Au overlayer thickness. Because of this blue shift in $\lambda_{initial}$, with increasing Au layer thickness, etalons undergo smaller total shifts since all etalons deswell the same absolute amount because they are all made from exactly the same microgels (note that spectra for all Au overlayer thicknesses all end ±10 nm from each other). In fact, the change is so apparent that from the 5 nm overlayer to the 35 nm overlayer, a shift of over 50 nm is lost. Therefore, to achieve the maximum sensitivity, as well as the fastest response time, a microgel etalon sensor with a thin Au overlayer is needed.

dx.doi.org/10.1021/jp207138f |J. Phys. Chem. B 2011, 115, 14359–14368

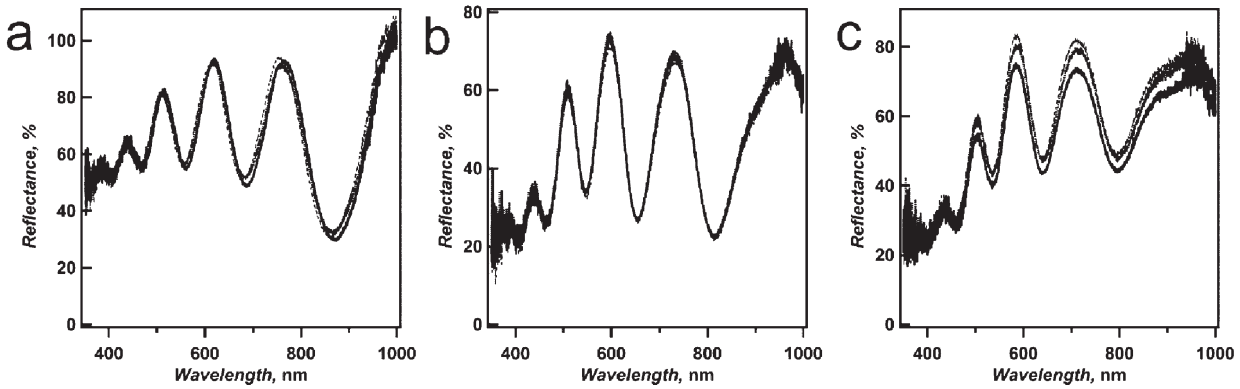

Figure 7. Initial spectra for multiple deswelling runs done on three different etalons with overlayer thicknesses of (a) 5 nm, (b) 15 nm, and (c) 25 nm. The initial spectrum for each run is plotted as follows: (solid), run 1; (· · ·), run 2; and (— — —), run 3.

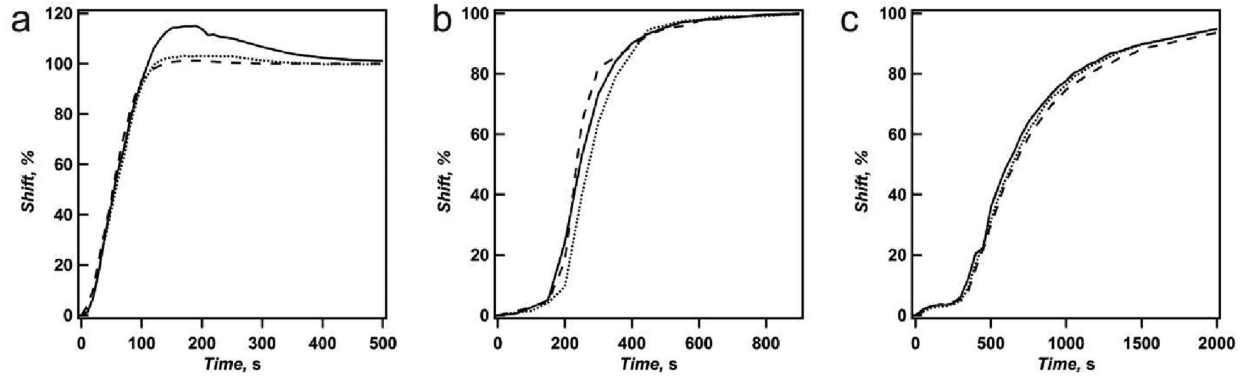

Figure 8. Percent shift as a function of time for three successive deswelling runs for etalons with (a) 5 nm, (b) 15 nm, and (c) 25 nm Au overlayers. The curves reveal that no significant change in kinetics occurs with multiple deswelling runs. Deswelling run number is represented as follows: run 1, (solid); run 2, (· · ·); and run 3, (— — —). The initial reflectance spectra for each run are presented in Figure 7 and show that no significant changes in the spectrum exist after deswelling.

Solvent Exchange Mechanism. There are three possible mechanisms by which the microgels in the etalon are accessible to the external solvent. An analyte can enter the microgel layer, and solvent can be exchanged as follows: (1) exclusively through the edges; (2) exclusively through the Au overlayer; or (3) through a combination of diffusion through both the edges and the overlayer. The data suggests that the preferred route of solvent exchange with the microgel layer is through the overlayer. We reach this conclusion based on the observation that the deswelling time and deswelling rate constants both decrease with Au overlayer thickness increases. This is accompanied by a concomitant decrease in the maximum deswelling rate (Figures 3 and 5). Additionally, the lag and plateau phase times increase with increasing overlayer thicknesses (Figure 2). That is, thicker Au overlayers are less porous, hindering solvent exchange through the overlayer, hence slowing the deswelling process down.[29,30,38] This suggests that the solvent exchange mechanism transitions from a state that is predominantly through the overlayer to one that proceeds less through the overlayer and more through the sides. By studying the diffusion of small molecules through polymers, Pant and Boyd show that as the free volume of the polymer decreases, the diffusion of small molecules through the polymer necessarily slows.[39−41] Therefore, we conclude that diffusion through the edges of a microgel etalon must be a slow process due in part to packing effects and confinement, as compared to diffusion through pinholes in the Au overlayer.[42] However, at the thickest of overlayers, the deswelling response is never entirely halted, again suggesting that exchange through the edges is partially operative.

To further show that the solvent exchange mechanism transitions from a state that is less through the overlayer and more through the sides of the film, we evaluated the deswelling kinetics as a function of the substrate size. If, for thick overlayers, the solvent exchange is occurring through the sides of the etalon, then the time it takes for the solvent to fully exchange into and out of the microgel layer should decrease with decreasing substrate size, resulting in faster deswelling kinetics. We can further assume that the majority of the kinetics is defined by the solvent exchange through the Au overlayer or the confined polymer film because microgel deswelling kinetics are known to be fast due to their relatively small size.[43−46] To conduct this experiment, the deswelling response for a single etalon needs to be observed multiple times as the substrate size is systematically varied (decreased), and the kinetics for the different size etalons are compared. Before comparisons can be made, the effect that mulitple deswellings/reswellings have on etalon kinetics needs to be determined.

Etalons with overlayer thicknesses of 5, 15, and 25 nm were deswollen multiple times by the introduction of the MeOH solution, as above. We verified that microgel etalons could be

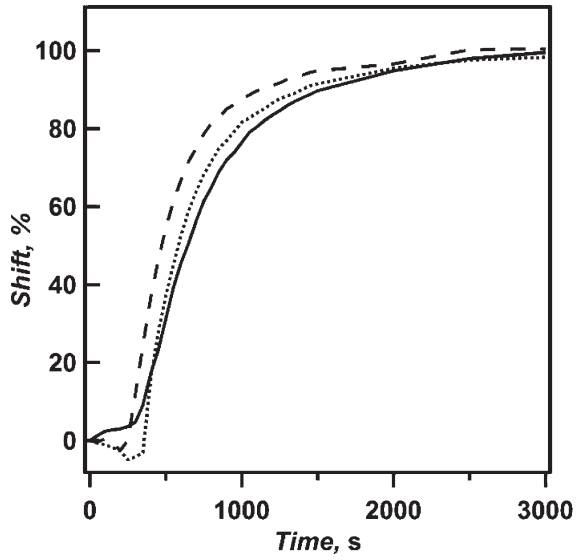

Figure 9. Percent shift as a function of time illustrating the effect of etalon size on deswelling kinetics for an etalon with a 25 nm Au overlayer and an area of (solid) 6.25 cm^2, (···) ~2.5 cm^2, and (– – –) ~0.9 cm^2.

returned to their initial state following a deswelling by following the rinsing/soaking protocol described in the Experimental Section. Figure 7 shows that the initial spectra all closely match one another before and after deswelling. Figure 8 shows the results for multiple deswellings of the individual etalons. It can be seen that no appreciable systematic change in the deswelling behavior of the etalons was observed, implying that if the Au overlayer is being affected in some way by deswelling, it is not changing the kinetic response.

Given that multiple deswelling runs have minimal effect on the kinetics, the deswelling kinetics for a single etalon of different dimensions were probed. An etalon from set 2 with a 25 nm Au overlayer of dimensions 6.25 cm^2 (2.5 cm × 2.5 cm) was deswollen. This overlayer thickness was chosen because it is likely that near 25 nm, the Au begins to act more like a bulk film, and the pore size is significantly reduced,[29,30] resulting in solvent exchange through the sides of the film. The sample was rinsed and soaked five times with deionized water and then cut to approximately 2.5 cm^2 (~1.0 cm × ~2.5 cm) and deswollen a second time. Next, it was rinsed and soaked, cut to approximately ~0.9 cm^2 (~0.9 cm × ~1.0 cm) and deswollen a third time. The deswelling curves for these smaller substrates, together with a deswelling curve for the full-sized substrate (run number two from Figure 8c) are shown in Figure 9. When the etalon was made slightly smaller (~2.5 cm^2), little change in the rate or total time that it took to deswell was observed. However, when it was cut to ~0.9 cm^2, the etalon reached 100% deswollen significantly faster than other larger substrates. The lag phase for the smallest etalon is also significantly reduced; this etalon begins to deswell faster and reaches its maximum kinetic rate of deswelling sooner. We hypothesize that this is a result of the shorter distance that the solvent needs to travel to afford a response.

Taken together, data from experiments on etalons with different overlayer thicknesses as well as data from an etalon of different sizes reveals the mechanism by which etalons exchange with their solvent and thus take up an analyte of interest. A microgel etalon will exchange its solvent primarily through the Au overlayer; however, there is a measurable decrease in the time that the smaller etalon takes to actuate when the overlayer is relatively thick. This suggests that there is solvent exchange through the edges as the overlayer becomes less porous and more like a bulk film, affecting the response kinetics.

In order to build microgel etalons that are responsive to a variety of stimuli or to employ microgel etalons as temperature tunable optical filters, an understanding of this kinetic response is necessary. Thinner Au overlayers afford a strikingly faster deswelling rate as compared to thicker overlayers, which take significantly more time to fully deswell. They also provide sharper reflectance peaks and greater total shifts (higher sensitivity) when compared to etalons with thick Au overlayers. This information will be imperative to future sensing endeavors where a fast response with high sensitivity is desired.

CONCLUSIONS

The mechanism by which microgel etalons exchange their solvent was probed by deswelling etalons with different Au overlayer thicknesses. An analyte (in this study, MeOH) must first diffuse to the sensing area, and the microgel's water of solvation must exit the etalon. Data for the kinetics of deswelling of etalons with various Au overlayer thicknesses in response to a $MeOH/H_2O$ solution strongly suggests that etalons exchange with their solvent through both the top and through the edges. However, the route of exchange through the Au overlayer is greatly favored, and an increase in overlayer thickness slows the rate of deswelling. To create functional POC etalon sensors that respond to various stimuli, a thinner overlayer affording a fast kinetic response would be ideal. However, other applications, e.g., drug delivery, may require longer response times. Therefore, an understanding of etalon response kinetics is a fundamentally important question for both applications and full comprehension of microgel-based materials.

ASSOCIATED CONTENT

Supporting Information. A photograph of the experimental setup and AFM images for the thickness analysis. This material is available free of charge via the Internet at http://pubs.acs.org.

AUTHOR INFORMATION

Corresponding Author
*E-mail: michael.serpe@ualberta.ca.

ACKNOWLEDGMENT

M.J.S. acknowledges funding from the University of Alberta (the Department of Chemistry and the Faculty of Science), the Natural Science and Engineering Research Council (NSERC), the Canada Foundation for Innovation (CFI), and the Alberta Advanced Education & Technology Small Equipment Grants Program (AET/SEGP). M.J.S acknowledges Mark McDermott for the use of the thermal evaporator and Ryan Fuierer (Asylum Research) for providing AFM tips. M.C.D.C. would like to acknowledge NSERC for an Undergraduate Student Research Award.

REFERENCES

(1) Yager, P.; Domingo, G. J.; Gerdes, J. *Annu. Rev. Biomed. Eng.* **2008**, *10*, 107.
(2) Mabey, D.; Peeling Rosanna, W.; Ustianowski, A.; Perkins Mark, D. *Nat. Rev. Microbiol.* **2004**, *2*, 231.
(3) Tudos, A. J.; Besselink, G. J.; Schasfoort, R. B. *Lab Chip* **2001**, *1*, 83.
(4) Delouise, L. A.; Fauchet, P. M.; Miller, B. L.; Pentland, A. A. *Adv. Mater.* **2005**, *17*, 2199.
(5) Bonanno, L. M.; DeLouise, L. A. *Adv. Funct. Mater.* **2010**, *20*, 573.
(6) Norman, R. J.; Lowings, C.; Chard, T. *Lancet* **1985**, *1*, 19.
(7) Alexeev, V. L.; Sharma, A. C.; Goponenko, A. V.; Das, S.; Lednev, I. K.; Wilcox, C. S.; Finegold, D. N.; Asher, S. A. *Anal. Chem.* **2003**, *75*, 2316.
(8) Chan, S.; Horner, S. R.; Fauchet, P. M.; Miller, B. L. *J. Am. Chem. Soc.* **2001**, *123*, 11797.
(9) Chan, S.; Fauchet, P. M.; Li, Y.; Rothberg, L. J. *Proc. SPIE* **2000**, *3912*, 23.
(10) Holtz, J. H.; Asher, S. A. *Nature* **1997**, *389*, 829.
(11) Choi, S. Y.; Mamak, M.; von Freymann, G.; Chopra, N.; Ozin, G. A. *Nano Lett.* **2006**, *6*, 2456.
(12) Kurt, P.; Banerjee, D.; Cohen, R. E.; Rubner, M. F. *J. Mater. Chem.* **2009**, *19*, 8920.
(13) O'Brien, P. G.; Puzzo, D. P.; Chutinan, A.; Bonifacio, L. D.; Ozin, G. A.; Kherani, N. P. *Adv. Mater.* **2010**, *22*, 611.
(14) Tsuji, S.; Kawaguchi, H. *Langmuir* **2005**, *21*, 8439.
(15) Brooker, G. *Modern Classical Optics*; Oxford University Press: Oxford, U.K., 2003.
(16) Vaughan, J. M. *The Fabry-Perot Interferometer: History, Theory, Practice and Applications*; Taylor & Francis Group: New York, 1989; pp 583.
(17) Kang, C.; Kim, E.; Baek, H.; Hwang, K.; Kwak, D.; Kang, Y.; Thomas, E. L. *J. Am. Chem. Soc.* **2009**, *131*, 7538.
(18) Lotsch, B. V.; Ozin, G. A. *Adv. Mater.* **2008**, *20*, 4079.
(19) Sorrell, C. D.; Carter, M. C. D.; Serpe, M. J. *Adv. Funct. Mater.* **2011**, *21*, 425.
(20) Sorrell, C. D.; Carter, M. C. D.; Serpe, M. J. *ACS Appl. Mater. Interfaces* **2011**, *3* (4), 1140–1147.
(21) Sorrell, C. D.; Serpe, M. J. *Adv. Mater.* **2011**, *23*, 4088.
(22) Pelton, R. H.; Chibante, P. *Colloids Surf.* **1986**, *20*, 247.
(23) Jones, C. D.; Lyon, L. A. *Macromolecules* **2000**, *33*, 8301.
(24) Blackburn, W. H.; Lyon, L. A. *Colloid Polym. Sci.* **2008**, *286*, 563.
(25) Hoare, T.; Pelton, R. *Macromolecules* **2007**, *40*, 670.
(26) Kim, J.; Singh, N.; Lyon, L. A. *Biomacromolecules* **2007**, *8*, 1157.
(27) Gawel, K.; Stokke, B. T. *Soft Matter* **2011**, *7*, 4615.
(28) Meng, Z.; Smith, M. H.; Lyon, L. A. *Colloid Polym. Sci.* **2009**, *287*, 277.
(29) Norrman, S.; Andersson, T.; Peto, G.; Somogyi, S. *Thin Solid Films* **1981**, *77*, 359.
(30) Golan, Y.; Margulis, L.; Rubinstein, I. *Surf. Sci.* **1992**, *264*, 312.
(31) Winnik, F. M.; Ottaviani, M. F.; Bossmann, S. H.; Garcia-Garibay, M.; Turro, N. J. *Macromolecules* **1992**, *25*, 6007.
(32) Winnik, F. M.; Ringsdorf, H.; Venzmer, J. *Macromolecules* **1990**, *23*, 2415.
(33) Schild, H. G.; Muthukumar, M.; Tirrell, D. A. *Macromolecules* **1991**, *24*, 948.
(34) Anac, I.; Aulasevich, A.; Junk, M. J. N.; Jakubowicz, P.; Roskamp, R. F.; Menges, B.; Jonas, U.; Knoll, W. *Macromol. Chem. Phys.* **2010**, *211*, 1018.
(35) McPhee, W.; Tam, K. C.; Pelton, R. *J. Colloid Interface Sci.* **1993**, *156*, 24.
(36) Wohlfarth, C. Refractive Index of the Mixture (1) Water; (2) Methanol. In *Data Extract from Landolt-Börnstein III/47: Optical Constants*; Lechner, M. D., Ed.; Springer-Verlag: Berlin Heidelberg, 2008; Vol. 47.
(37) Openhaim, G.; Grushka, E. *J. Chromatogr., A* **2002**, *942*, 63.
(38) Roland, T.; Khalil, A.; Tanenbaum, A.; Berguiga, L.; DelichËre, P.; Bonneviot, L.; Elezgaray, J.; Arneodo, A.; Argoul, F. *Surf. Sci.* **2009**, *603*, 3307.
(39) Pant, P. V. K.; Boyd, R. H. *Macromolecules* **1993**, *26*, 679.
(40) Pant, P. V. K.; Boyd, R. H. *Macromolecules* **1992**, *25*, 494.
(41) Boyd, R. H.; Pant, P. V. K. *Macromolecules* **1991**, *24*, 6325.
(42) Yelash, L.; Virnau, P.; Binder, K.; Paul, W. *Phys. Rev. E: Stat., Nonlinear, Soft Matter Phys.* **2010**, *82*, 050801/1.
(43) Tanaka, T.; Fillmore, D. J. *J. Chem. Phys.* **1979**, *70*, 1214.
(44) Okajima, T.; Harada, I.; Nishio, K.; Hirotsu, S. *J. Chem. Phys.* **2002**, *116*, 9068.
(45) Li, Y.; Tanaka, T. *Annu. Rev. Mater. Sci.* **1992**, *22*, 243.
(46) Shibayama, M.; Tanaka, T. *Adv. Polym. Sci.* **1993**, *109*, 1.